Experimental Results and Performance Analysis of a 500 m/sec Linear Induction Launcher (LIL)

Z. Zabar, X.N. Lu, E. Levi, L. Birenbaum, and J. Creedon*
Polytechnic University, 333 Jay St., Brooklyn, NY 11201

* US Army ET&D Laboratory, Fort Monmouth, NJ 07703

Abstract: A computer model, previously validated, was used to study the performance of an experimental 3-phase launcher energized by a capacitor bank and designed to impart to a 137-gram projectile a muzzle velocity of 500 m/s: (1) the build-up of the traveling wave was examined; (2) the connection of the drive coils was changed; (3) the resistances of the drive circuits were calculated and measured; (4) the effect of the conductivity of the cylindrical tube (sleeve) constituting the projectile was assessed.

Experimentally, a doubling of the muzzle velocity was achieved, from an earlier-obtained 250 m/s, to its present 476 m/s. This was done by strengthening the thin-walled aluminum sleeve by heat-treatment (aging) to prevent it from being crushed when the input energy was raised to its design value.

1. Introduction

A linear induction launcher (LIL) is composed of two principal parts: the barrel, consisting of a linear array of coils, energized in polyphase fashion so as to create a traveling wave; and the projectile, consisting of a thin-walled aluminum cylinder (sleeve). The LIL is energized by discharging capacitors through the coils. Capacitance values are chosen to resonate with the inductance of the coils at a frequency which increases along the barrel, from breech to muzzle, so as to increase the velocity of the traveling wave as it advances toward the muzzle, driving the projectile through the launcher. Propelling and centering forces are created, simultaneously, by the interaction between the traveling wave magnetic field and the system of currents induced into the sleeve. The increase in frequency is obtained stepwise by dividing the barrel into sections which are energized sequentially [1-5], and this results in a reduction of the number of capacitors and switches.

A LIL prototype system (Model 3), designed to achieve a 500 m/s muzzle velocity, was built to provide scaling-up guidelines for the engineering of a full-scale system. It consists of a barrel, composed of a 60-cm-long array of 18 coils, of which 6 form the first section, and 12 the second section, with a 5 cm bore; and of a projectile, made of 1.6-mm-thick aluminum tubing, weighing 137 grams, and 20 cm long [1,2]. Many tests and studies were performed on Model 3 in the last two years. One major problem that had to be solved was misfiring of the switches, due to electromagnetic interference. Once this was resolved, the projectile was able to attain a muzzle velocity of 250 m/s [1]. However, this was too low, since 250 m/s was expected to be the value of the exit velocity from the first section alone. It was felt that the maximum speed attained by the projectile in the first section, 170 m/s, and hence its speed of entry into the second section, was inadequate, and was the principal factor that prevented proper additional acceleration from being imparted to it during its subsequent passage through the launcher. Attempts to obtain higher velocities by raising the capacitor voltage in the first section to the design value were unsuccessful, because the projectile was invariably crushed by the electromagnetic forces.

Recently, this difficulty was resolved sufficiently to allow us to safely raise the capacitor voltage in the first section from its previous maximum value of 3.7 kV, up to 3.9 kV. This was sufficient to raise the velocity of exit from the first section to 200 m/s, and the corresponding muzzle velocity to 476 m/s. Details are given in the sections to follow.

Computer simulation studies reported here show that it should even be possible to obtain a somewhat higher muzzle velocity, and that the energy stored in the capacitors could be even more efficiently utilized. These studies are based mainly on lumped-parameter circuit theory, and the calculations are performed using a mesh-matrix analysis technique [3-7]. Studies of the build-up of the currents in the drive coils indicate that, for a short period after the firing of the gun, the integrity of the traveling wave is maintained to a good degree, although it is somewhat distorted by the mutual inductance between adjacent drive coils. The effects of changes in the firing sequence, and of changes in the coil connections, are studied, and compared with the original arrangement, with the goal of making the best traveling wave. As a result of an anomalously-large damping of the coil currents, and hence of the traveling wave, a number of tests were carried out to find the total resistance of the drive circuit. Also studied are the effect of the resistance of the drive circuits, and of the conductivity of the sleeve projectile, on the muzzle velocity. Details of these studies, and the results, are presented below.

2. Achievement of a 476 m/s velocity from Model 3

Achievement of a muzzle velocity of 476 m/s resulted from an improvement of the mechanical strength and the electrical conductivity of the sleeve. The sleeve is made of aluminum 2024-T3. This material is not pure aluminum [8]; rather, it is an alloy containing many other metals, principally copper and magnesium (~4.5% and 1.5% by weight). At the suggestion of Ian Stone and David Haugh of the Research Defence Agency of the UK, the sleeve material was aged; i.e., it was heated at 170° C for 19-20 hours. Empirically, it was found that this combination gave the largest increase in strength, as measured by an increase in the Brinell hardness, of 12%. This made it possible to drive the projectile harder without crushing it, and enabled us to reach a much higher velocity. Heat-treating the sleeve not only increased its hardness, but also increased its conductivity from $1.56 \cdot 10^7$ to $2.0 \cdot 10^7$ S/m. Another important factor is that the kinetic energy transfer ratio from the capacitors to the projectile increased, for two reasons: (1) the higher conductivity of the sleeve reduced the Joule losses, and (2) the higher exit velocity from the first section decreased the slip, and therefore increased the efficiency of the second section.

Manuscript received May 1, 1994
This work was sponsored by the BMDO/IST and managed by US Army SDC under contract DASG60-91-C-015

Summarized in Table 1 below are the operating conditions of the launcher for the muzzle velocity of 476 m/s. The second section was fired at the end of a pre-set time interval, empirically determined, after the first section was fired (1.4 ms).

Table 1: Launcher operating conditions

	C [μF per phase]	*f* [Hz]	cap. V [kV]	*v* [m/sec]
1st section	1,200	1,250	3.9	200
2nd section	130	2,600	17	476

The muzzle velocity was measured with the aid of a fiber-optic guide bundle, which directed a beam of light across the muzzle end of the barrel to a detector. By displaying the detector output on the screen of a storage oscilloscope, it was possible to measure the length of time Δt that beam reception was interrupted. The muzzle velocity was calculated as (projectile length / Δt).

Measurements were made of the muzzle velocity when the second-section capacitor voltage was varied from 0 – 17 kV, and the first-section voltage was held constant at 3.9 kV. The results are shown as the solid curve in Fig. 1. For comparison, the predictions from the computer code are shown as the dashed curve. Agreement is seen to be quite close. The discrepancies are believed to be due mainly to the fact that, in the computer simulation, the drive circuit resistance is assumed to be constant, whereas it actually depends on the current, because of the presence of the ignitron switches. In this connection, it is noted that the muzzle velocity is strongly dependent on the drive circuit resistance. In the present simulation, lower values were used than in the companion paper [9] to account for the higher current, and this leads to the prediction of higher muzzle velocities.

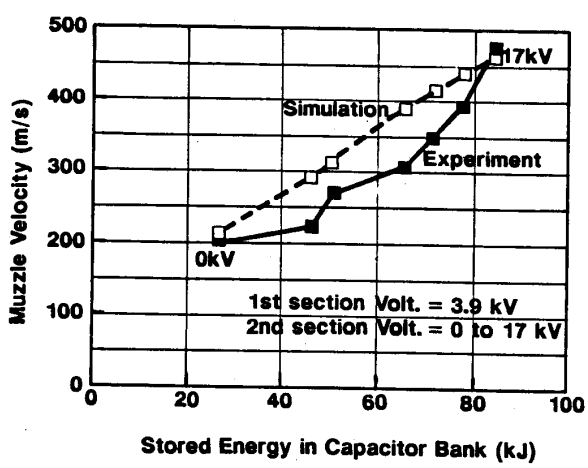

Fig. 1: Velocity vs. total energy stored in the capacitor bank

As reported earlier [1], to validate our computer code, the voltage oscillations across the capacitors of the first and second sections were observed on an oscilloscope, and compared with those calculated from our code using the actual launcher dimensions and voltages as input data. Very good agreement was obtained between experiment and predictions.

Figure 2(a) shows (from the computer simulation) velocity as a function of distance, and 2(b) shows force as a function of distance. The small force and the corresponding plateau in the velocity just before energization of the second section are due to (1) the strong decay in the barrel currents and (2) the fact that the length of the first section is the same as that of the sleeve, so that an increasing portion of the latter finds itself in the second section, which has not yet been energized.

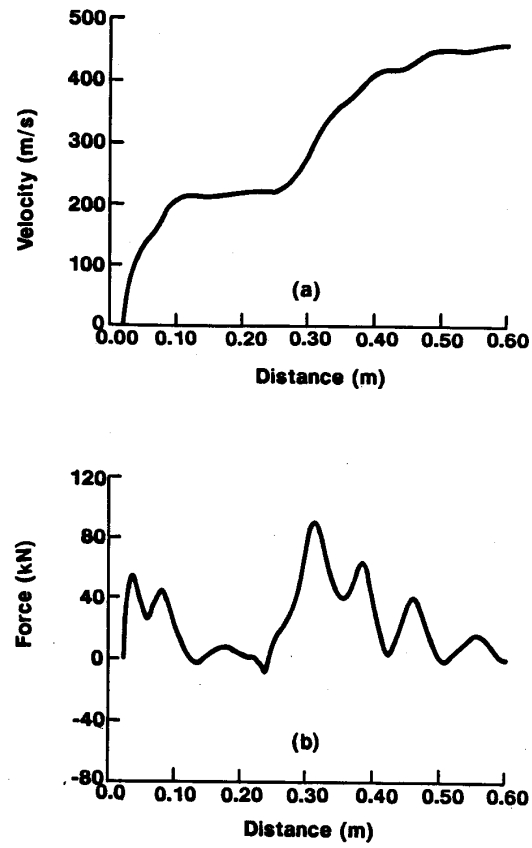

Fig. 2: Velocity (a) and force (b) as a function of the distance

3. Study of the build-up of the traveling wave

The waveforms of the voltages across the three capacitors of the second section of Model 3 LIL (Ref. [1], and see also Fig. 3 below) show that there are two main departures from an ideal traveling wave: (1) the large damping of the wave, especially for phase A, and (2) frequency mixing [10,11]. The main causes for this distortion are the mutual inductances between adjacent drive coils and with the sleeve. These points are discussed in detail below.

3.1 Effect of mutual inductance between adjacent drive coils

The amplitude of the phase A voltage in the first section decays much faster than that of phase B or phase C (see Sect. 3.2 below). Two ways for phase A to lose energy faster than the other two phases are: (1) more energy is transferred into the sleeve, and (2) energy is transferred to adjacent coils due to mutual inductance.

Figure 3 shows the current waveform of phase A in the second section for four cases, as obtained by computer simulation:
(1) only phase A is fired with no sleeve inside the barrel;
(2) only phase A is fired with sleeve inside the barrel;
(3) three phases are fired with no sleeve inside the barrel;
(4) three phases are fired with sleeve inside the barrel.

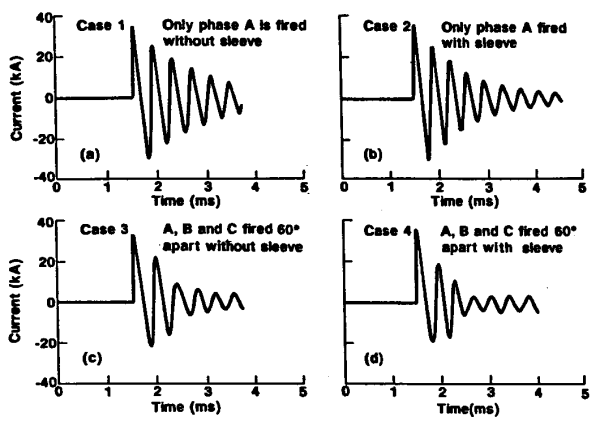

Fig. 3: Current in phase A of the second section (a) case 1, (b) case 2, (c) case 3, (d) case 4

From Fig. 3, it appears that the weakest damping occurs in case (1); damping is stronger in cases (2) and (3), and strongest in case (4). In case (1), in which current flows only in the coils of phase A, and the sleeve is absent, damping due to dissipation in the drive circuit is clearly demonstrated. In case (2), on the other hand, where the sleeve is present, damping of the phase A current is more rapid, indicating additional losses. These may be accounted for by energy transfer to the sleeve. In case (3), again the sleeve is absent, but all three phases have been fired at 60° intervals. Damping of the phase A current is seen to be quite strong; comparable, in fact, to that of case (2). Since the losses here evidently exceed those due to dissipation in the drive coils, an additional loss mechanism must be present. A simple explanation is that the voltages induced in the coils of phases B and C, due to the current in phase A, cause current to flow there once the switches of B and C are closed. Hence mutual inductance between windings of the different phases can account for energy transfer out of phase A coils. In case (4), in which the sleeve is again present, it is seen that the damping, and hence the losses, exceed those of case (3). This suggests that the additional losses are caused by energy transfer to the sleeve.

From the above computer simulation, one can also see that the frequency decreases with time. The highest frequency is in case (2). The lowest frequency is in case (3), and the frequencies for cases (1) and (4) are almost equal. Because of the mutual inductances between the barrel and the projectile, and between the adjacent drive coils, there may be expected to be a few different frequencies present in the system.

3.2 Optimization of the traveling wave

As a first simulation study, the time intervals between the firing of the three phases were varied. The phase delay for a balanced three-phase system is 120° in A, B, and C as shown in Fig. 4(a). In order to build up the traveling wave as quickly as possible and alleviate the single phasing problem, the three phases A, -C, and B are normally fired with a 60° delay, as shown in Fig. 4(b).

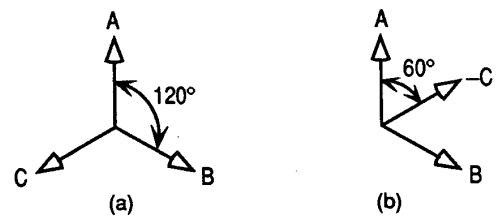

Fig. 4: Phasor diagrams (a) 120° delay (b) 60° delay

Computer simulation results show that the best delay is 60° (firing sequence is A, –C, and B). With this delay, we have the best three-phase current waveforms and the maximum muzzle velocity (see Table 2, line 1). This also suggests that the combination of damped L,C oscillations and polyphase excitation do indeed generate a traveling wave.

Table 2. Muzzle velocities for various coil connections

No	Firing sequence and coil connection	Velocity [m/s] in 1st section	Velocity [m/s] in 2nd section
1	A, –C, and B; (60°); series connection	173	250
2	AA, –CC, and BB; (60°); series connection	163	246
3	A, B, and C; (120°); series connection	153	241
4	A, –C, and B (60°); parallel connection	170	249

This result was confirmed by one experiment with the first section of Model 3 LIL, a heavier projectile (175 grams), and 3 kV voltage on the capacitor bank. When the firing sequence was 0°, 70°, 100°, the velocity obtained was 77 m/s, instead of 85 m/s, when the firing sequence was 60°.

As a second simulation study, we changed the connection of the drive coils from A, –C, and B to AA, –CC, and BB with a 60° delay. The width of the coils for one phase thus was doubled. The effect is to increase the coupling with the sleeve and to reduce the mutual inductance between drive

coils of different phases, thus increasing their equivalent self-inductance and reducing the frequency by 10% (see Table 2, line 2).

In a third study, the three phases were energized in the sequence A, B, C with a 120° delay (see Table 2, line 3).

As a fourth simulation study, parallel connection of the drive coils was tried, instead of the usual series connection. In order to keep the same amount of stored energy and the same frequency in the system, the capacitance was increased and the voltage on the capacitor was reduced (see Table 2, line 4).

For each of these four cases, the exit velocity from section one and the muzzle velocity were calculated. Also, in each case, the initial position in each section was optimized (only a slight adjustment was needed) so as to obtain the maximum velocity .

Some details of the performance with these four different connections are now compared with one another. (This work was done before we learned about aging of the sleeve.) Figure 5 shows the three-phase current waveforms in the first section for each case. With the AA, −CC, BB connection, as expected, the frequency mixing problem is alleviated. In the other three cases, once the new phase comes in, a new frequency is injected. All these connections introduce large harmonic components in the space distribution of the magnetic field. For the parallel connection, two traces are seen for each phase, since the currents in the two branches are unequal. This is so because, in the case of phase A, coils 1 and 4 are not similarly located with respect to the sleeve, which, at the start, is only partially in the core of coil 1, but wholly within coil 4.

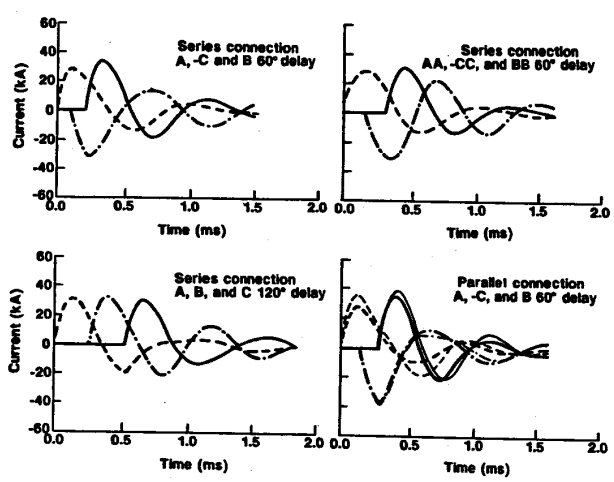

Fig. 5: Current waveforms for different connections and different firing sequences in the first section

Figure 6 compares the barrel and sleeve currents and force waves at t= 0.4 ms when the sleeve is in the first section for both the AA, −CC, BB, and the A, −C, B connections. One can see that the waveforms of the barrel and sleeve currents for the A, −C, B connection most closely resemble sinusoidal waves.

It is interesting to note that the change in velocity for these four cases is not very large. When looking at Fig. 7, which shows force as a function of time for these four cases in the first section, it is seen that the areas under each force curve are almost the same. Some of them have larger peak values and narrow areas, and some of them have wider areas and lower peak values. The connection A, −C, B is preferred. When it is necessary to reduce the voltage level on the capacitor bank, the parallel connection is more advantageous.

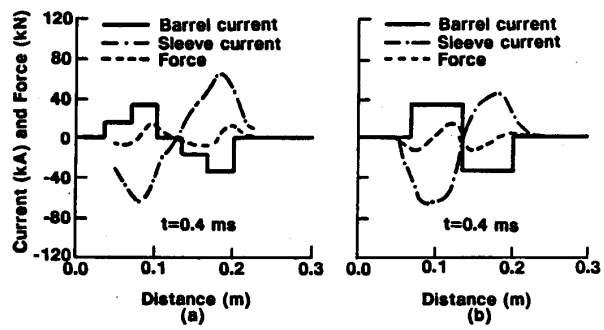

Fig. 6: Current and force distributions for (a) A, -C, B and (b) AA, BB, CC connections

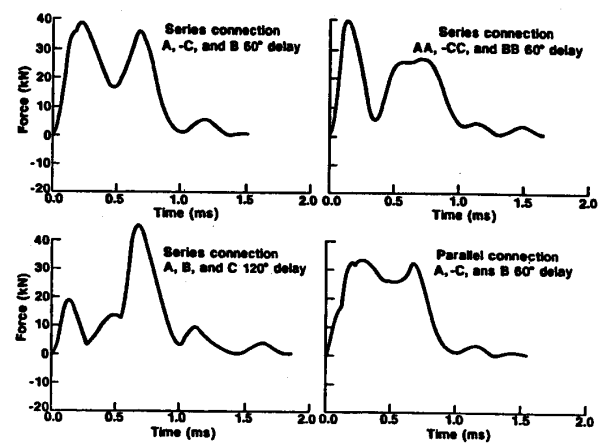

Fig. 7: Force as a function of time for different connections and different firing sequences in the first section

4. Study of resistivity of the system

4.1 Tests and estimate of resistance of the drive circuit

In our launcher, each drive circuit is an oscillatory RLC circuit. Experiments in which only the coils of a single phase were energized, and with the sleeve absent (as in Section 2,

above) showed an unexpectedly large damping in the drive circuit current. This, in turn, required much more energy storage in the system in order to get the design velocity. The equivalent resistance was measured experimentally by determining the time constant for the decay of the voltages across the capacitors. Since they were expected to decay exponentially, the decay constant α was determined as $\alpha = \frac{1}{t_2 - t_1} \ln\left(\frac{V_1}{V_2}\right) = \frac{R}{2L}$, where V_1 and V_2 are the positive or negative peaks of the drive voltage, and t_1 and t_2 are the times at which they occur. From the experimental data, we obtained the decay time constant; then the resistance was calculated from $R = 2\alpha L$, where L is the impedance-bridge-measured self-inductance of each phase. This varies with the connection of the drive coils. Figure 8 shows the voltages in phase A of the second section with the different connections shown in Fig. 9. Although the distance between each coil of one phase is 10 cm, one can see that there still exists enough mutual inductance between the coils to make a significant difference in the waveform and frequency.

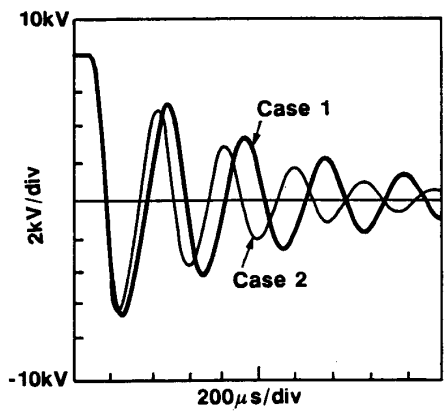

Fig. 8: Voltage waveforms for different connections of the drive coils in phase A in the second section

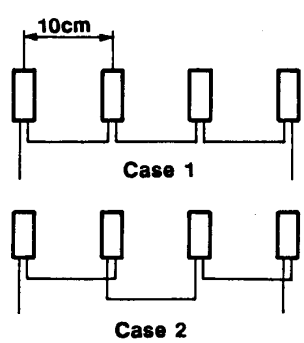

Fig. 9: The different connections of the drive coils in phase A in the second section

It is possible that longitudinal iron bars, part of the structure that holds the drive coils in alignment, may enhance the mutual inductance between coils. The total equivalent resistance for each phase will be equal to the average value of the resistance derived from the measured values of α with different connections using for the inductance four times the inductance of a single coil.

The total resistance of one phase of the drive circuits as calculated for the first section and for the second section are shown in Table 3. (Note that the first section has two series-connected coils per phase, while the second section has four, and that the type of capacitor in the second section is different from the one in the first section.)

Table 3. Resistance of drive circuits

	1st section 3.5 kV	2nd section 12 kV
Resistance per coil	4 mΩ	4 mΩ
Resistance of phase A	18 mΩ	55 mΩ
Resistance of phase B	17.6 mΩ	55.6 mΩ

The measured resistance for each drive coil is only 2 mΩ; including the connection wires, it is about 4 mΩ. Therefore, the large circuit resistance must be due to either the ignitron or the capacitors. With regard to the ignitron (NL 488A), it is very difficult to assess its resistance under transient conditions because of its dependence on the current. According to the manufacturer (National Electronics Inc., Illinois), the resistance of the ignitron is relatively small.

The remainder of the resistance must come from the capacitor. This is a high-energy-density capacitor which uses, as electrodes, very thin metallized deposits on the dielectric material. This thin metallized sheet may produce the unwanted large resistance. Another cause may be the insulation material. The solution for this problem is to replace the capacitors. The types of high voltage (HV) capacitors presently available and their losses are shown in Table 4. (HD designates high-energy-density capacitor; D is the dissipation factor ωCr, where r is equivalent series resistance of the capacitor C; ε_r is the relative dielectric constant of the insulating material.)

Table 4. Characteristics of HV capacitors (f = 1.0 kHz)

	Paper/oil	Mylar	Poly-propylene	PVDF HD
D	0.3 - 0.4 %	0.1 - 0.5 %	0.01 - 0.02 %	5 - 15 %
ε_r	2.2	3	2.7	8 - 12

These capacitors may also be made with aluminum foil electrodes, that give much lower losses. The PVDF (poly vinylidene fluoride) capacitors are the newest high-energy-density capacitors. However they allow no voltage reversal at all (i.e., 0% reversal). Probably, the best for our purposes are polypropylene, aluminum foil capacitors since their dissipation factor is the lowest.

4.2 Effect of conductivity of projectile on muzzle velocity

As in an induction motor, one expects that there exists a value of resistance of the projectile at which a maximum force, and hence a maximum muzzle velocity, is obtained. As was already mentioned, the conductivity of our aluminum projectile without aging was $1.56 \cdot 10^7$ S/m, and $2.0 \cdot 10^7$ S/m with aging. The corresponding resistances of the sleeve (i.e., the resistance of one of the 20 coils into which the 20-cm long sleeve is assumed to be divided) are 0.2 mΩ and 0.16 mΩ without and with aging of the sleeve. By changing the conductivity of the projectile, different exit velocities in the first and the second sections are obtained, as shown in Table 5. In this table, R is equal to 0.16 mΩ.

The capacitors were the same as in the 250 m/s testing and simulation (i.e. the same power supply as in Table 1, except that the voltage on the capacitor of the first section is 3.8 kV and 15 kV for the second section). It appears that the velocities are strongly dependent on the resistance of the sleeve, and that the resistance with aging, by coincidence, gives the best results.

Table 5. Effect of projectile resistance on velocity

	Resistance of one projectile coil	Velocity (m/sec) 1st/2nd section
1	10 × R	138/179
2	5 × R	150/221
3	2 × R	167/220
4	1.1 × R	177/250
5	R = 0.16 mΩ	190/330
6	0.7 × R	163/243

5. Conclusion

Although the traveling wave is distorted by mutual inductances, single phasing, and large damping in the drive circuit, the behavior of the launcher is still relatively insensitive to these factors. The LIL appears to have the same 'forgiving' character as a conventional induction motor. The best way to connect the drive coils of the barrel is A, –C , B with the three phases firing with a 60° delay. It is important to reduce the resistance of the drive circuit of the launcher in order to improve the performance. In a two-section launcher, the frequency is low and the length of each section is short. The performance of a multi-section high-velocity launcher is different from that of the two-section launcher. When the frequency gets higher and the length of each section increases, the performance of the launcher improves [see companion paper, Ref. 9]. The parallel connection of the drive coils in each phase is recommended for the high-frequency, high-voltage section.

6. Acknowledgment

The authors wish to express their thanks to Ian Stone and David Haugh of the UK Research Defence Agency for their valuable suggestion; Dr. J. L. He for his previous research work; and Mr. N. R. Goradia, Dr. K-B Kim, and Mr. S.-Y. Yoo for their contributions to the experimental work.

References

[1] Z. Zabar, X.N. Lu, L. Birenbaum, E. Levi and J.L. He, "A 500 m/s Linear Induction Launcher," 8th IEEE Pulsed Power Conference, San Diego, CA; June 17-19, 1991.

[2] Z. Zabar, X.N. Lu, J.L. He, L. Birenbaum, E. Levi, S. Kuznetsov and M.D. Nahemow, "Test Results for Three Prototype Models of a Linear Induction Launcher," IEEE Trans. on Magnetics, Vol. 27, No. 1, pp. 558-562, Jan. 1991.

[3] J. L. He, E. Levi, Zabar, L. Birenbaum, "Determination of the Parameters of Induction-Type EM Launchers," 7th IEEE Pulsed Power Conference, Monterey, California, June 12-14, 1989.

[4] J. L. He, Z. Zabar, E. Levi and L. Birenbaum, "Transient Performance of Linear Induction Launchers Fed by Generators and by Capacitor Banks," IEEE Trans. on Magnetics, Vol. 27, No. 1, pp 585-90, Jan. 1991.

[5] J. L. He, E. Levi, Z. Zabar, L. Birenbaum and Y. Naot, "Analysis of Induction-Type Coilgun Performance Based on Cylindrical Current Sheet Model," IEEE Trans. on Magnetics, Vol. 27, No. 1, pp 579-584, Jan. 1991.

[6] D.G. Elliott, "Mesh Matrix Analysis Method for Electromagnetic Launchers," IEEE Trans. on Magnetics, Vol. 25, No. 1, pp. 164-169, Jan. 1988.

[7] M.M. Widner, "WARP-10: A Numerical Simulation Model for the Cylindrical Reconnection Launcher", IEEE Trans. on Magnetics, Vol. 27, No. 1, pp. 634-638, Jan. 1991.

[8] "Aluminum Standards and Data", The Aluminum Association, Inc., Washington, DC, 1984, pp. 15, 93.

[9] X.N. Lu, Z. Zabar, E. Levi, and L. Birenbaum, "Transition Between Two Sections in a Linear Induction Launcher (LIL)," 7th Symposium on Electromagnetic Launcher Technology, San Diego, California, April 20-24, 1994.

[10] X. N. Lu, E. Levi, Z. Zabar, L. Birenbaum, and J. L. He, "Departures from Ideal Performance in the Linear Induction Launcher (LIL)," AIAA 30th Aerospace Sciences Meeting, Reno, Nevada, Jan. 6-9, 1992.

[11] X.N. Lu, E. Levi, Z. Zabar, and L. Birenbaum, "Behavior of Azimuthal Currents Induced in the Projectile of the Linear Induction Launcher," IEEE Trans. on Magnetics, Vol. 29, No. 1, pp. 696-700, Jan. 1993.